Robotic Subsurface Pipeline Mapping with a Ground-penetrating Radar and a Camera

Haifeng Li, Chieh Chou, Longfei Fan, Binbin Li, Di Wang, and Dezhen Song

Abstract— We propose a novel subsurface pipeline mapping method by fusing Ground Penetrating Radar (GPR) scans and camera images. To facilitate the simultaneous detection of multiple pipelines, we model the GPR sensing process and prove hyperbola response for general scanning with non-perpendicular angles. Furthermore, we fuse visual simultaneous localization and mapping outputs, encoder readings with GPR scans to classify hyperbolas into different pipeline groups. We extensively apply the J-Linkage method and maximum likelihood estimation to improve algorithm robustness and accuracy. As the result, we optimally estimate the radii and locations of all pipelines. We have implemented our method and tested it in physical experiments with representative pipeline configurations. The results show that our method successfully reconstructs all subsurface pipes. Moreover, the average estimation errors for two orientation angles of pipelines are $0.81°$ and $0.72°$, respectively. The average localization error is 4.69cm.
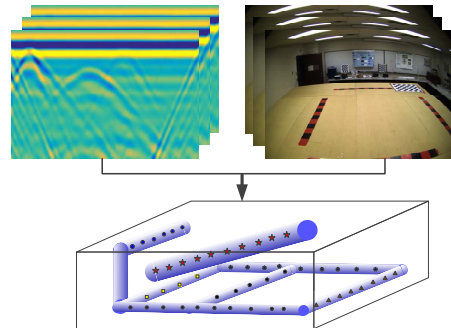
Fig. 1. An illustration of our subsurface pipeline mapping problem. Given a set of GPR scans and camera images, our algorithm outputs a set of collinear center axis points and radii of all buried pipelines.

I. Introduction

Precise 3D maps for underground pipelines, such as gas, water, and sewage pipes, are important for local governments, utility companies, and civil engineers. However, underground pipeline locations in old urban areas are usually unknown. Even in new urban areas, there are no 3D maps but a rough 2D layout information [1] for subsurface pipelines. As a result, civil construction projects can easily damage underground pipes and cause significant loss. A Ground penetrating radar (GPR) is an important tool for the detection and localization of underground objects. However, a GPR does not directly provide a 3D position but convoluted and noisy radar reflection images which require trained eyes to manually recognize objects of interest. For pipeline mapping, the traditional GPR methods have too many limitations and constraints: only allow one pipeline in survey area, require prior knowledge of pipe diameter or orientation, and perpendicular scanning with respect to the pipe. Therefore, the whole process is labor intensive and costly.

H. Li and L. Fan are with CS Department, Civil Aviation University of China, Tianjin, 300300, China, and also with Fujian Provincial Key Laboratory of Information Processing and Intelligent Control, Minjiang University, Fuzhou, 350108, China. Email: *hfli@cauc.edu.cn*.

D. Song, C. Chou, B. Li, and D. Wang are with CSE Department, Texas A&M University, College Station, TX 77843, USA. Emails: *dzsong@cse.tamu.edu*, *cchou@tamu.edu*, and *binbinli@tamu.edu*.

To automate the pipeline mapping problem, we propose a new method to simultaneously map multiple subsurface pipelines using a GPR and a camera (see Fig. 1). We model the GPR sensing process and prove/derive hyperbola responses for general scanning with non-perpendicular angles. This allows us to develop a new hyperbola detection algorithm for multiple pipeline detection. Next we fuse visual simultaneous localization and mapping (vSLAM) outputs and encoder readings with GPR scans to classify hyperbolas into groups belonged to different pipelines. We extensively apply the J-Linkage method and the maximum likelihood estimation (MLE) to improve algorithm robustness and accuracy. As the result, we optimally estimate the radii and locations of all pipelines. We have implemented our method and tested it in physical experiments. The results show that our method successfully reconstructs all subsurface pipes. Moreover, the average estimation errors for two orientation angles of pipelines are $0.81°$ and $0.72°$, respectively. The average localization error is 4.69cm.

II. Related Work

Pipeline mapping is a critical step for assessing the condition of the buried utility pipelines. There are many existing efforts focusing on condition assessment [2] in general. Popular approaches include electromagnetic, acoustic, and seismic methods. An UK project named Mapping the Underworld (MTU) [3] focuses on locating, mapping, and recording buried utility assets by fusing multiple sensors.

Among different sensor modalities, GPRs have been widely used in subsurface target detection [4], [5]. However, mapping the underground targets from GPR signals is nontrivial, because a GPR does not provide 3D positions

but a reflection image with high degrees of freedom (DoFs) for interpretation. Windsor et al. [6] estimate subsurface pipe diameters with a given radio propagation velocity. Al-Nuaimy et al. [7] estimate pipeline depth by assuming zero pipeline radius and a perpendicular scanning trajectory. The assumptions limit their methods to cases when the pipeline is buried very deep and with small radius. To deal with this limitation, many methods [8], [9] simultaneously estimate the wave velocity and pipe radii. However, the perpendicular scanning constraint remains which is difficult to be satisfied in real world applications. Recently, Li et al. [10] propose an approach to estimate features of the buried pipelines without the requirement of perpendicular scanning. However, only an approximate model is proposed and the approach has not considered multiple pipeline case.

A GPR generates hyperbola response when perpendicularly scanning over a cylindrical object. Pipeline mapping is actually the detection and analysis of hyperbolas. The commonly used hyperbola detection methods include conic fitting method [11], machine learning-based method [12], [13], and Hough transform-based method [14]. Most conic fitting methods can only identify one conic in each image and are often sensitive to outliers. Although the probabilistic hyperbola mixture model [15] is proposed to deal with these problems, the data partition in noisy GPR images before hyperbola fitting is still problematic. Results from machine learning methods depend on the quality of manually-labeled training sets for different settings which are difficult to obtain in applications. Hough transform-based methods need to repeat with different parameter combinations to search the best hyperbola, and are quite time-consuming. Furthermore, it is difficult to specify a suitable threshold for the number of votes to determine the number of hyperbolas in the process. To deal with these problems, our method builds on a new GPR sensing model, the fusion of vSLAM, encoder, and GPR, and integration of J-Linkage and MLE. The approach does not require prior knowledge about the total number of hyperbolas or pipelines.
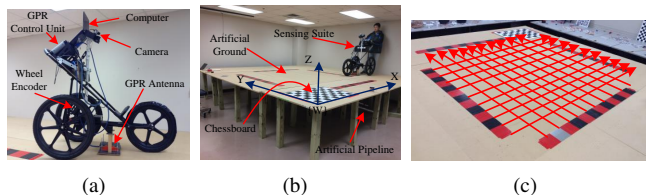

Fig. 2. (a) Our sensing suite on a tricycle, (b) experiment setup, and (c) grid based scanning pattern contains two parallel groups that are perpendicular to each other.

To map multiple pipelines, the 3D location of the detected pipelines need to be geo-registered to a spatial referencing system for further filtering. Combining GPR and GPS is posed in recent work [10]. However, GPS signals are often challenged in urban environments. Chen and G. Cohn [16] propose a pipeline mapping approach by fusing GPR detection results with existing utility records. However, the method inherently depends on both the quality and the availability of utility records. Our method employs a fixed on-board camera to localize itself and the GPR based on vSLAM technique [17], which requires minimal to zero prior knowledge and is less restricted by environments.

Our group has worked on both surface and subsurface infrastructure inspection using a robotic sensing suite for several years [18]. The sensing suite contains a camera and a GPR. We have calibrated the extrinsic parameters between the GPR and the camera using a mirror-assisted method [19]. Furthermore, we have employed the customized artificial landmarks and pose graph optimization method to fulfill the synchronization task [20], which lays a foundation for this work.

III. PROBLEM FORMULATION

Fig. 2(a) illustrates our sensing suite design which mounts a GPR and a camera on a tricycle. To focus on the horizontal pipeline mapping, we have the following assumptions.

a.1 All pipelines can be approximated as piecewise connected cylinders whose centerlines intersect the horizontal plane with an angle less than 45 degrees, since a GPR cannot distinguish pipes that are close-to-vertical and most pipeline segments are horizontal anyway.

a.2 The sensing suite moves on a flat ground plane, and

a.3 Pipelines are buried in a homogeneous medium, and the radio wave propagation velocity is priorly known from calibration.

During scanning, the GPR transmitting antenna sends polarized high-frequency radio waves into soil (see Fig. 3(a)). When reaching a target with different electromagnetic properties than its surrounding medium, the wave is reflected back and then the microwave traveling time from GPR transmitter to object to receiver is recorded which forms an A-scan (Fig. 3(b)). Based on assumption a.3, the traveling time can be converted into the traveling distance. While the GPR moves on the ground to perform scanning, it produces a series of A-scans at different positions. This ensemble of A-scans forms a B-scan [21] (Fig. 3(c)). A collection of B-scans combining with images captured by the camera at different scanning positions serve as inputs. To describe them, we define the following notations,

- $\{W\}$, the 3D world coordinate system with X-Y plane representing the horizontal ground plane, and Z-axis pointing to the upward direction (see Fig. 3(d)). A 3D point in $\{W\}$ is denoted as $\mathbf{X}^W \in \mathbb{R}^3$.
- $A_q^k = \{a_s | s = 1, \ldots, n_q\}$, the j-th A-scan belonging to the k-th B-scan, with $a_s > 0$ denoting the reflection amplitude of the s-th sample point.
- $B_k = \{A_q^k | q = 1, \ldots, n_k\}$, the k-th B-scan consisting of n_k A-scans. Each B-scan can be viewed as a 2D image, where each $A_q^k \in B_k$ is a column of pixels. Note that this 2D GPR image is in an Euclidean coordinate because each pixel position $\mathbf{x} = [x_k, d_k]^\mathrm{T} \in \mathbb{R}^2$ is in physical units of meters with x_k-axis parallel to the GPR moving direction, representing the distance traveled, and d_k-axis indicating the distance from GPR
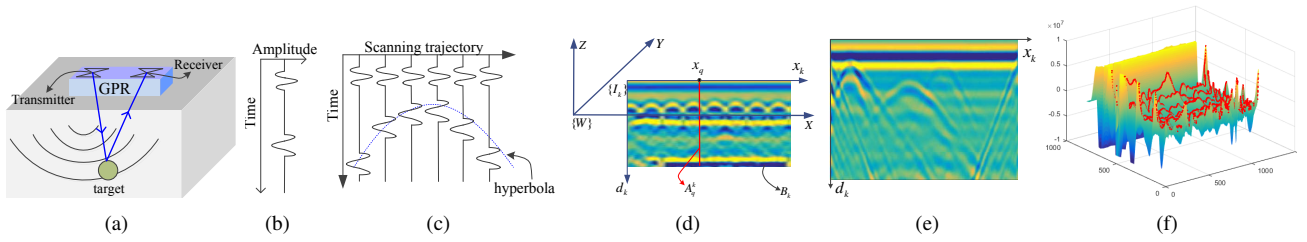
Fig. 3. An illustration of GPR working principle and coordinate system. (a-c) a ball shaped object registers itself as a hyperbola in B-scan. (d) coordinate systems and important notations. (e) A typical B-scan 2D view. (f) Sample B-scans 3D view with peaks marked by combining parallel scanning results.
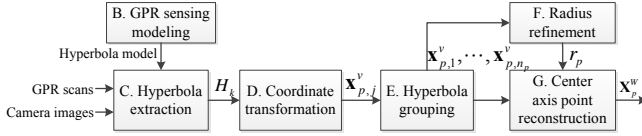

Fig. 4. System diagram. Each box index letter corresponds to the subsection number in Section IV.

to object. Its origin is at the position of the first A-scan in B_k (see Fig. 3(d)).

- $H_k = \{\mathbf{H}_j | j = 1, \ldots, n_h\}$, the set of hyperbolas extracted from B_k, with each $\mathbf{H}_j, 1 \leq j \leq n_h$ being the parameter vector of a hyperbola.
- $\mathbf{L}_p = [r_p, (\mathbf{X}_{p,1}^W)^{\mathrm{T}}, \ldots, (\mathbf{X}_{p,n_p}^W)^{\mathrm{T}}]^{\mathrm{T}}$, the p-th pipeline segment with its radius equal to r_p, $\mathbf{X}_{p,j}^W, j = 1, \ldots, n_p$ representing the j-th reconstructed point in $\{W\}$.
- $\Omega = \cup\{\mathbf{L}_p\}$, the detected pipeline set.

Our pipeline mapping problem is defined as follows,

Definition 1: Given synchronized camera images and GPR B-scans, extract hyperbola set H_k from each B_k, obtain Ω.

IV. ALGORITHM

Our system diagram is shown in Fig. 4. The system inputs are the synchronized GPR scans and camera images. We derive a sensing model which establishes hyperbola-shaped radar signals when the GPR scans a straight pipeline along a linear trajectory. The model allows us to extract hyperbolas from each B_k. Fused with vSLAM and encoder readings, the detected hyperbola vertexes in all B_k's are transformed into $\{W\}$. Then our algorithm classifies hyperbolas into different groups according to their residing pipelines. Finally, for each pipeline group, we estimate pipe radius and locations. We begin with the data collection step.

A. Data Collection on Grid

Both the GPR and the camera are fixed on a sensing suite (see Fig. 2(c)) which moves along a straight line to collect data. To guarantee the reconstruction accuracy, it is necessary to ensure that the intersection angle between the scanning trajectory and pipeline center lines projected to the horizontal plane is between $45°$ and $90°$. Therefore, we scans using a grid pattern consisting of evenly spaced survey lines in two parallel groups with perpendicular directions for pipeline mapping (see Fig. 2(c)). It is obvious that we must have one group with the intersection angle is no less than $45°$ even

we do not know actual pipe orientation. This group can be easily identified in GPR readings. Hence, we assume all data are from this group in the rest of the paper, which means all B_k's are taken from parallel scans. Next let us model the GPR sensing process in a single scan.

B. GPR Sensing Modeling

According to [8], horizontal cylindrical pipelines are recognized as hyperbolas in GPR scans. We explain it using a simple case when the GPR scans a pipeline perpendicularly before extending it to general cases with unknown orientations.

1) Perpendicular Scanning: Fig. 5(a) illustrates this ideal case. Let d_i be the distance measurement by the GPR at point x_i in B_k, x_v denote the closest point to the pipeline on the scanning trajectory along x_k-axis, and d_v denote the measured distance from x_v to the pipeline. The geometric relationship between the extracted hyperbola in B_k and the pipeline radius r is governed by the red right triangle formed at location x_v according to [22],

$$(d_i + r)^2 = (x_i - x_v)^2 + (d_v + r)^2. \qquad (1)$$

We can rewrite (1) as the canonical hyperbola formulation,

$$\frac{(d_i + r)^2}{(d_v + r)^2} - \frac{(x_i - x_v)^2}{(d_v + r)^2} = 1. \qquad (2)$$

In fact, the point $[x_v, d_v]^{\mathrm{T}}$ is the hyperbola vertex. However, in practice, the accurate orientation of pipelines is unknown. The probability of having a perpendicular scanning is negligible. A generic linear trajectory (GLT) usually does not have a known approaching angle to the pipeline centerline. We need a sensing model for a GLT. More importantly, we need to know if the signal shape in the B-scan is still a hyperbola.

2) GLT Sensing Model: Fig. 5(b) illustrates that a GPR scans a pipeline along a GLT. Two angles, α and θ, are employed to describe the orientation of a straight pipeline segment where α is the angle between the projection of the pipeline centerline on the X-Y plane of $\{W\}$ (i.e. ground plane) and the GLT, and θ is the angle between the pipeline and the GLT. Denote $\mathbf{X}_i$ and $\mathbf{X}_v$ as two 3D points on GLT in $\{W\}$ and $\mathbf{X}_v$ is the closest point to the pipeline. The measured distances from $\mathbf{X}_i$ and $\mathbf{X}_v$ by the GPR are d_i and d_v, respectively. The following lemma presents the GPR sensing model when crossing the pipeline with a GLT.
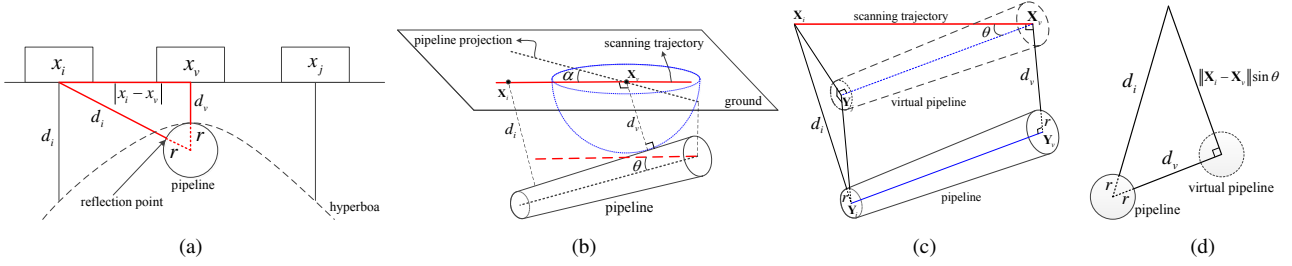
Fig. 5. Understanding GPR sensing model: (a) perpendicular scanning, (b) a GLT scanning, (c) virtual pipeline, and (d) 2D projection of (c).

Lemma 1: When the GPR scans the subsurface pipeline along a GLT, the resulting signal in B-scan is the following hyperbola,

$$\frac{(d_i + r)^2}{(d_v + r)^2} - \frac{(x_i - x_v)^2 (\sin \theta)^2}{(d_v + r)^2} = 1, \tag{3}$$

where x_i and x_v denote the x-coordinate values in B_k when the GPR is located at $\mathbf{X}_i$ and $\mathbf{X}_v$, respectively.

Proof: Fig. 5(b-d) illustrates the GLT scanning case. Denote $\overline{\mathbf{XY}}$ as the line segment connecting 3D points $\mathbf{X}$ and $\mathbf{Y}$. We select two 3D points $\mathbf{Y}_v$ and $\mathbf{Y}_i$ lying on the centerline of the pipeline, such that $\overline{\mathbf{X}_v \mathbf{Y}_v} \perp \overline{\mathbf{Y}_v \mathbf{Y}_i}$ and $\overline{\mathbf{X}_i \mathbf{Y}_i} \perp \overline{\mathbf{Y}_v \mathbf{Y}_i}$. Thus,

$$\|\overline{\mathbf{X}_v \mathbf{Y}_v}\| = d_v + r$$
$$\|\overline{\mathbf{X}_i \mathbf{Y}_i}\| = d_i + r.$$

We introduce a virtual pipeline $\overline{\mathbf{X}_v \mathbf{Y}_j}$ which is parallel to $\overline{\mathbf{Y}_v \mathbf{Y}_i}$ (see Fig. 5(c)). Then, the angle between $\overline{\mathbf{X}_v \mathbf{X}_i}$ and $\overline{\mathbf{X}_v \mathbf{Y}_j}$ is θ, thus $\|\overline{\mathbf{X}_i \mathbf{Y}_j}\| = \|\overline{\mathbf{X}_v \mathbf{X}_i}\| \sin \theta$.

Since $\overline{\mathbf{X}_v \mathbf{Y}_v} \perp \overline{\mathbf{Y}_v \mathbf{Y}_i}$ and $\overline{\mathbf{Y}_v \mathbf{Y}_i} \parallel \overline{\mathbf{X}_v \mathbf{Y}_j}$, thus $\overline{\mathbf{X}_v \mathbf{Y}_v} \perp \overline{\mathbf{X}_v \mathbf{Y}_j}$. Additionally, $\overline{\mathbf{X}_v \mathbf{Y}_v} \perp \overline{\mathbf{X}_v \mathbf{X}_i}$, thus $\overline{\mathbf{X}_v \mathbf{Y}_v}$ is perpendicular to the plane where $\mathbf{X}_v$, $\mathbf{X}_i$ and $\mathbf{Y}_j$ are lying on. Therefore, $\overline{\mathbf{X}_v \mathbf{Y}_v} \perp \overline{\mathbf{X}_i \mathbf{Y}_j}$. Since $\overline{\mathbf{X}_v \mathbf{Y}_v} \parallel \overline{\mathbf{Y}_i \mathbf{Y}_j}$, we can obtain $\triangle \mathbf{X}_i \mathbf{Y}_i \mathbf{Y}_j$ is a right triangle. Projecting the scanning scenario into 2D view (see Fig. 5(d)), we have

$$(d_i + r)^2 = \left(\|\mathbf{X}_i - \mathbf{X}_v\| \sin \theta\right)^2 + (d_v + r)^2. \tag{4}$$

Since both $|x_i - x_v|$ and $\|\mathbf{X}_i - \mathbf{X}_v\|$ represent the same GPR traveling distance, we have $|x_i - x_v| = \|\mathbf{X}_i - \mathbf{X}_v\|$. Rewriting (4) in canonical hyperbola format, Lem. 1 is proved. ∎

Lem. 1 shows that the resulting B-scan signals from scanning a pipeline along a GLT is still a hyperbola. Therefore, we can utilize this knowledge to extract them from noisy B-scans.

C. Hyperbola Extraction

The raw GPR data must be preprocessed before extracting hyperbolas. The pre-processing involves time-zero correction, average background subtraction, and low pass filtering. In B_k, the intensity of each pixel $\mathbf{x} = [x_k, d_k]^{\mathrm{T}}$ represents the sum of the radar reflections from all underground objects whose distances to x_k are equal to d_k. For each A-scan in B_k, we extract all peak points with local highest intensities, since only peak points are potential hyperbola

points. Define $\mathbf{x}_i$ be the i-th peak point in B_k. Denote $M_k = \{\mathbf{x}_i | i = 1, \ldots, n_m\}$ as the set of extracted peak points. Thus, our hyperbola detection problem is, given M_k, to detect multiple hyperbolas. Extracting hyperbolas from a GPR B-scan is non-trivial due to multiple solutions and significant noises as shown in Figs. 3(e) and 3(f).

To find all hyperbolas, we apply the J-linkage [23] framework to detect them from each GPR B-scan. The J-linkage approach can simultaneously fit multiple models to data corrupted by noise and outliers without specifying model number. Let us define $\mathbf{x}_{j,i} = [x_{j,i}, d_{j,i}]^{\mathrm{T}}$ be the i-th point lying on the j-th hyperbola in B_k. Specially, we denote $[x_{j,v}, d_{j,v}]^{\mathrm{T}}$ as the vertex of the hyperbola $\mathbf{H}_j$. We can represent the hyperbola form in Lem. 1 as,

$$\tilde{\mathbf{x}}_{j,i}^{\mathrm{T}} \mathbf{Q}_j \tilde{\mathbf{x}}_{j,i} = 0, \tag{5}$$

where $\tilde{\mathbf{x}}_{j,i} = [x_{j,i}, d_{j,i}, 1]^{\mathrm{T}}$ is the homogeneous coordinate of $\mathbf{x}_{j,i}$, and

$$\mathbf{Q}_j = \begin{bmatrix} (\sin \theta)^2 & 0 & -x_{j,v}(\sin \theta)^2 \\ 0 & -1 & -r \\ -x_{j,v}(\sin \theta)^2 & -r & (\sin \theta)^2 x_{j,v}^2 + d_{j,v}^2 + 2d_{j,v}r \end{bmatrix}$$

A generic conic, $ax^2 + bxy + cy^2 + dx + ey + f = 0$, has 5 DoFs. However, there are only 4 DoFs in our conic in (5) since the major axis of each hyperbola in B-scan is vertical which means $b = 0$. Thus, we can parameterize each hyperbola as $\mathbf{H}_j = [x_{j,v}, d_{j,v}, \sin \theta, r]^{\mathrm{T}}$. Four points lying on the hyperbola are sufficient to compute a minimal solution of this hyperbola by solving (5).

In the J-linkage process, we first randomly choose M minimal sample set of 4 peak points to estimate the initial hyperbola by solving (5). For each initial hyperbola, if it satisfies $x_{j,v} > 0$ and $d_{j,v} > 0$, which indicates the vertex of the hyperbola lying in the first quadrant of B_k, we consider it as a model hypothesis. Otherwise, we discard it.

For the rest, we follow the standard J-linkage steps which generate multiple clusters. For each cluster $\mathcal{M}_j$, if its size is greater than a threshold N_h, we accept this model hypothesis and further refine it from all peak points in $\mathcal{M}_j$. We model $\mathbf{x}_{j,i}$'s measurement error as a zero mean Gaussian with covariance matrix $\sigma_{j,i}^2 \mathbf{I}_2$, where $\mathbf{I}_2$ is a 2×2 identity matrix. Stacking all points in $\mathcal{M}_j$ together, we obtain the following

overall measurement error function,

$$C_h(\mathbf{H}_j) = \begin{bmatrix} \tilde{\mathbf{x}}_{j,1}^{\mathrm{T}} \mathbf{Q}_j \tilde{\mathbf{x}}_{j,1} \\ \vdots \\ \tilde{\mathbf{x}}_{j,m_j}^{\mathrm{T}} \mathbf{Q}_j \tilde{\mathbf{x}}_{j,m_j} \end{bmatrix}, \qquad (6)$$

where $m_j = |\mathcal{M}_j|$ denotes the total point number in $\mathcal{M}_j$.

The MLE of $\mathbf{H}_j$ can be obtained by minimizing the Mahalanobis distance,

$$\mathbf{H}_j^* = \underset{\mathbf{H}_j}{\arg\min}\, C_h(\mathbf{H}_j)^{\mathrm{T}} \textstyle\sum_{H,j}^{-1} C_h(\mathbf{H}_j), \qquad (7)$$

where $\sum_{H,j} = diag(\sigma_{j,1}^2,\ldots,\sigma_{j,m_j}^2)$ is a diagonal matrix. This nonlinear optimization problem can be solved using Levenberg-Marquardt(LM) algorithm. Also, it is not difficult to obtain the covariance matrix of the estimated $\mathbf{H}_j^*$ using error propagation methods in Chapter 5 of [24].

From $\mathbf{H}_j^*$, we can obtain the hyperbola vertex. Let us define $\mathbf{v}_{p,j}^I = [x_{j,v}, d_{j,v}]^{\mathrm{T}}$ to be the vertex of the j-th hyperbola generated from the p-th pipeline in the image coordinate system of B_k. Next we need to classify and group the extracted hyperbolas in $\{W\}$ according to its pipe. This requires fusing with vSLAM and encoder readings.

D. Sensor Fusion for Coordinate Transformation

We project all hyperbola vertexes onto the X-Y plane of $\{W\}$. Define $\mathbf{x}_{p,j}^v = [x_{p,j}^v, y_{p,j}^v]^{\mathrm{T}}$ to be the corresponding position on X-Y plane in $\{W\}$ where the GPR receives $\mathbf{v}_{p,j}^I$. Here, we use the superscript v to indicate the vertex. We know $\mathbf{v}_{p,j}^I$ in B_k but finding $\mathbf{x}_{p,j}^v$ requires combining vSLAM outputs and wheel encoder data.

We denote the starting and ending points of the scanning line as $\mathbf{x}_{s,k} = [x_{s,k}, y_{s,k}]^{\mathrm{T}}$ and $\mathbf{x}_{e,k} = [x_{e,k}, y_{e,k}]^{\mathrm{T}}$, respectively, which are measured by vSLAM algorithm. Note that they are 2D because all points are in X-Y plane with $z = 0$. We do not directly use $\mathbf{x}_{s,k}$ and $\mathbf{x}_{e,k}$ to localize $\mathbf{x}_{p,j}^v$ due to the vSLAM measurement errors. Since the GPR moves along a group of parallel GLTs according to Section IV-A, we adopt the parallelism constraint to refine $\mathbf{x}_{s,k}$ and $\mathbf{x}_{e,k}$. Denote $\hat{\mathbf{x}}_{s,k}$ and $\hat{\mathbf{x}}_{e,k}$ as the estimations of $\mathbf{x}_{s,k}$ and $\mathbf{x}_{e,k}$, respectively. Let us define $\mathbf{p}_v = [(\hat{\mathbf{x}}_{s,1})^{\mathrm{T}}, \ldots, (\hat{\mathbf{x}}_{s,n})^{\mathrm{T}}, \mathbf{v}]^{\mathrm{T}}$ to be the parameter vector, where $\mathbf{v}$ is 2×1 directional vector with $\|\mathbf{v}\| = 1$, denoting the moving direction of all parallel trajectories, and n is total number of the parallel trajectories. Define l_k to be the length of the k-th linear trajectory, which is obtained from wheel encoder readings. Thus,

$$\hat{\mathbf{x}}_{e,k} = \hat{\mathbf{x}}_{s,k} + l_k \mathbf{v}. \qquad (8)$$

We model both the covariance matrices of $\mathbf{x}_{s,k}$ and $\mathbf{x}_{e,k}$ as a zero mean Gaussian with covariance matrix $\sigma_v^2 \mathbf{I}_2$, where $\mathbf{I}_2$ is a 2×2 identity matrix. We estimate $\hat{\mathbf{x}}_{s,k}, k = 1, \ldots, n$
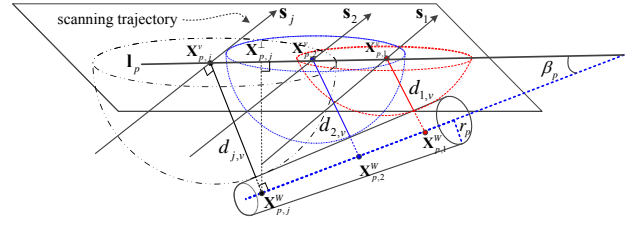

Fig. 6. An illustration of pipeline localization under parallel GLTs.

and $\mathbf{v}$ by minimizing the following cost function

$$C_v(\mathbf{p}_v) = \begin{bmatrix} \hat{\mathbf{x}}_{s,1} - \mathbf{x}_{s,1} \\ \vdots \\ \hat{\mathbf{x}}_{s,n} - \mathbf{x}_{s,n} \\ \hat{\mathbf{x}}_{s,1} + l_1\mathbf{v} - \mathbf{x}_{e,1} \\ \vdots \\ \hat{\mathbf{x}}_{s,n} + l_n\mathbf{v} - \mathbf{x}_{e,n} \end{bmatrix}. \qquad (9)$$

We obtain the MLE of $\mathbf{p}_v$ by solving the following optimization problem,

$$\mathbf{p}_v^* = \underset{\mathbf{p}_v}{\arg\min}\, C_v(\mathbf{p}_v)^{\mathrm{T}} \textstyle\sum_v^{-1} C_v(\mathbf{p}_v), \qquad (10)$$

where $\sum_v = diag(\sum_{s,1}, \ldots, \sum_{s,n}, \sum_{e,1}, \ldots, \sum_{e,n})$ is a block-wise diagonal matrix, $\sum_{s,k}$ and $\sum_{e,k}$ denote the covariance matrices of $\mathbf{x}_{s,k}$ and $\mathbf{x}_{e,k}$, respectively. Here we ignore the measurement errors from the wheel encoder because the wheel encoder is very accurate when the sensing suite moves on flat ground.

With $\hat{\mathbf{x}}_{s,k}$ and $\hat{\mathbf{x}}_{e,k}$ obtained, we can obtain each hyperbola vertex position $\mathbf{x}_{p,j}^v$ in $\{W\}$ using the wheel encoder. We already know the wheel encoder increments between $\mathbf{x}_{p,j}^v$ and $\hat{\mathbf{x}}_{s,k}$ to be $x_{j,v}$. We also know the wheel encoder increments between $\hat{\mathbf{x}}_{s,k}$ and $\hat{\mathbf{x}}_{e,k}$ as $\|\hat{\mathbf{x}}_{e,k} - \hat{\mathbf{x}}_{s,k}\|$. Thus, the position of $\mathbf{x}_{p,j}^v$ is determined as,

$$\mathbf{x}_{p,j}^v = \left(1 - \frac{x_{j,v}}{\|\hat{\mathbf{x}}_{e,k} - \hat{\mathbf{x}}_{s,k}\|}\right)\hat{\mathbf{x}}_{s,k} + \frac{x_{j,v}}{\|\hat{\mathbf{x}}_{e,k} - \hat{\mathbf{x}}_{s,k}\|}\hat{\mathbf{x}}_{e,k}. \quad (11)$$

Again, the covariance matrix of the estimated $\mathbf{x}_{p,j}^v$ can be obtained using error propagation methods in Chapter 5 of [24].

E. Hyperbola Grouping

Knowing hyperbola vertexes in $\{W\}$ allows us to classify hyperbolas from multiple B_k's into different groups according to their residing pipelines. This allows us to simultaneously detect multiple pipelines. Recall that we perform scanning by following parallel GLTs (see Fig. 6). Let $\mathbf{s}_j, j = 1, \ldots, n_p$ represent the parallel GLTs crossing the p-th pipeline, thus we have $\mathbf{s}_1 \parallel \mathbf{s}_2 \parallel \ldots \parallel \mathbf{s}_{n_p}$. Recall that $\mathbf{x}_{p,j}^v = [x_{p,j}^v, y_{p,j}^v]^{\mathrm{T}}$ is 2D point on X-Y plane of $\{W\}$ when the GPR receives the j-th hyperbola vertex $[x_{j,v}, d_{j,v}]^{\mathrm{T}}$ from the p-th pipeline, and $\mathbf{X}_{p,j}^W$ is the j-th center axis point on the p-th pipeline, which is the closest axis point to $\mathbf{s}_j$. The following lemma presents the geometric model for center axis point reconstruction.

Lemma 2: If the GPR scans the p-th pipeline along a set of parallel GLTs, $\mathbf{s}_j, j = 1, \ldots, n_p$, and produces the sequence of $\mathbf{x}_{p,j}^v, j = 1, \ldots, n_p$ where the hyperbola vertexes are perceived, as illustrated in Fig. 6, then all $\mathbf{x}_{p,j}^v, j = 1, \ldots, n_p$ are collinear to line $\mathbf{l}_p$, and the corresponding closest 3D center pipe axis points to each scanning GLT $\mathbf{s}_j$ can be computed as follows,

$$\mathbf{X}_{p,j}^W = \begin{bmatrix} (1 - \lambda_{p,j})\mathbf{x}_{p,j}^v + \lambda_{p,j}\mathbf{x}_{p,j-1}^v \\ -(d_{j,v} + r_p)\cos\beta_p \end{bmatrix}, \qquad (12)$$

where r_p denotes the radius of the p-th pipeline, β_p is the angle between $\mathbf{l}_p$ and the pipeline centerline, and $\lambda_{p,j} = \frac{(d_{j,v}+r_p)\sin\beta_p}{\|\mathbf{x}_{p,j}^v - \mathbf{x}_{p,j-1}^v\|}$.

Proof: According to the working principle of GPR, for each $\mathbf{s}_j$, the hyperbola vertex is generated by the reflection of the pipeline surface point which is closest to $\mathbf{s}_j$. Thus, with $d_{j,v}$ known in each $\mathbf{s}_j$, all possible reflection points of the pipeline constitutes a hemisphere centered at $\mathbf{x}_{p,j}^v$ with radius equal to $d_{j,v}$, as shown in Fig. 6. The pipeline is tangential with all hemispheres.

Denote $\mathbf{X}_{p,j}^v = [(\mathbf{x}_{p,j}^v)^{\mathrm{T}}, 0]^{\mathrm{T}}$ as the 3D coordinate of $\mathbf{x}_{p,j}^v$, and $\overline{\mathbf{XY}}$ as the line segment connecting 3D points $\mathbf{X}$ and $\mathbf{Y}$. For each $\mathbf{s}_j$, we have

$$\overline{\mathbf{X}_{p,j}^v \mathbf{X}_{p,j}^W} \perp \mathbf{s}_j \text{ and } \overline{\mathbf{X}_{p,j}^v \mathbf{X}_{p,j}^W} \perp \overline{\mathbf{X}_{p,1}^W \mathbf{X}_{p,n_p}^W}.$$

$$\mathbf{s}_1 \parallel \mathbf{s}_2 \parallel \ldots \parallel \mathbf{s}_{n_p}$$

$$\therefore \overline{\mathbf{X}_{p,1}^v \mathbf{X}_{p,1}^W} \parallel \ldots \parallel \overline{\mathbf{X}_{p,n_p}^v \mathbf{X}_{p,n_p}^W}.$$

$\therefore$ all $\overline{\mathbf{X}_{p,j}^v \mathbf{X}_{p,j}^W}, j = 1, \ldots, n_p$ are coplanar.
$\therefore$ all $\mathbf{x}_{p,j}^v, j = 1, \ldots, n_p$ are collinear.

With the line denoted as $\mathbf{l}_p$, it is clear that $\mathbf{l}_p$ and $\overline{\mathbf{X}_{p,1}^W \mathbf{X}_{p,n_p}^W}$ are coplanar and intersect to each other. Furthermore, due to all $\mathbf{s}_j, j = 1, \ldots, n_p$ are on the horizontal plane, the plane determined by $\mathbf{X}_{p,1}^W$, $\mathbf{X}_{p,j}^W$ and $\mathbf{X}_{p,j}^v$ is a vertical plane. Inside this vertical plane, there exists a vertical line passing $\mathbf{X}_{p,j}^W$ and intersecting $\mathbf{l}_p$ at point $\mathbf{X}_{p,j}^\perp$ (see Fig. 6).

Connecting line segment $\overline{\mathbf{X}_{p,j}^W \mathbf{X}_{p,j}^\perp}$, we have

$$\overline{\mathbf{X}_{p,j}^W \mathbf{X}_{p,j}^\perp} \perp \overline{\mathbf{X}_{p,j}^v \mathbf{X}_{p,j-1}^v}.$$

Using trigonometry, we have

$$\|\mathbf{X}_{p,j}^v - \mathbf{X}_{p,j}^\perp\| = (d_{j,v} + r_p)\sin\beta_p,$$

$$\mathbf{X}_{p,j}^\perp = (1 - \frac{(d_{j,v}+r_p)\sin\beta_p}{\|\mathbf{x}_{p,j}^v - \mathbf{x}_{p,j-1}^v\|})\mathbf{X}_{p,j}^v + \frac{(d_{j,v}+r_p)\sin\beta_p}{\|\mathbf{x}_{p,j}^v - \mathbf{x}_{p,j-1}^v\|}\mathbf{X}_{p,j-1}^v.$$

Since $\mathbf{X}_{p,j}^\perp$ and $\mathbf{X}_{p,j}^W$ have the same X and Y coordinates, replacing the third element of $\mathbf{X}_{p,j}^\perp$ with $-(d_{j,v}+r_p)\cos\beta_p$, Lem. 2 is proved. ∎

Lem. 2 implies that we can simultaneously detect multiple pipes by grouping the hyperbolas. It can be done by fitting multiple lines from the hyperbola vertex projection points. Again, J-linkage framework is applied. Define $\tilde{\mathbf{x}}_{p,j}^v = [x_{p,j}^v, y_{p,j}^v, 1]^{\mathrm{T}}$ to be the homogeneous form of $\mathbf{x}_{p,j}^v$. We denote $\mathbf{l}_p$ as the 2D line projected from the p-th pipeline on

X-Y plane of $\{W\}$. Any $\tilde{\mathbf{x}}_{p,j}^v$ generated from p-th pipeline satisfies the following equation,

$$(\tilde{\mathbf{x}}_{p,j}^v)^{\mathrm{T}}\mathbf{l}_p = 0. \qquad (13)$$

A minimal solution requires two points. The rest follows the standard J-Linkage approach. After classifying the hyperbolas into different groups where all hyperbolas in the same group are generated from the same pipeline, we are ready to reconstruct pipelines with the grouped hyperbolas.

F. Pipeline Radius Refinement

Hyperbolas in the same group belong to the same pipeline and share the same radius. We can use this to refine the estimation of radius. Denote $r_{p,j}, j = 1, \ldots, n_p$ as the estimated radius of the p-th pipeline using the j-th hyperbola by (7), with estimation variance σ_j^2. Define r_p to be the radius of the p-th pipeline. To estimate r_p optimally by combining all $r_{p,j}$'s, We define the following error function,

$$C_r(r_p) = \begin{bmatrix} r_p - r_{p,1} \\ \vdots \\ r_p - r_{p,n_p} \end{bmatrix}. \qquad (14)$$

The MLE of r_p can be obtained by solving the following optimization problem,

$$r_p^* = \arg\min_{r_p} C_r(r_p)^{\mathrm{T}}\textstyle\sum_{r,p}^{-1}C_r(r_p), \qquad (15)$$

where $\sum_{r,p} = diag(\sigma_1^2, \ldots, \sigma_{n_p}^2)$ is a diagonal matrix.

G. Pipeline Center Axis Point Reconstruction

The final step is to estimate points $\mathbf{X}_{p,j}^W$ on the pipe center axis. Lem. 2 shows that we can obtain them from $\mathbf{X}_{p,j}^v$, $\mathbf{l}_p$ and β_p. We use the geometric relationship to obtain them. Let us define the parameter vector to be estimated as $\mathbf{p} = [(\hat{\mathbf{X}}_{p,1}^v)^{\mathrm{T}}, \ldots, (\hat{\mathbf{X}}_{p,n_p}^v)^{\mathrm{T}}, (\mathbf{l}_p)^{\mathrm{T}}, \beta_p]^{\mathrm{T}}$, where $\hat{\mathbf{X}}_{p,j}^v, j = 1, \ldots, n_p$ denotes the estimation of $\mathbf{X}_{p,j}^v$. Recall that $\mathbf{X}_{p,j}^v = [(\mathbf{x}_{p,j}^v)^{\mathrm{T}}, 0]^{\mathrm{T}}$. Then, we estimate $\mathbf{p}$ by minimizing the following cost function,

$$C_p(\mathbf{p}) = \begin{bmatrix} \hat{\mathbf{X}}_{p,1}^v - \mathbf{X}_{p,1}^v \\ \vdots \\ \hat{\mathbf{X}}_{p,n_p}^v - \mathbf{X}_{p,n_p}^v \\ (\tilde{\mathbf{x}}_{p,1}^v)^{\mathrm{T}}\mathbf{l}_p \\ \vdots \\ (\tilde{\mathbf{x}}_{p,n_p}^v)^{\mathrm{T}}\mathbf{l}_p \\ \|\hat{\mathbf{X}}_{p,2}^v - \hat{\mathbf{X}}_{p,1}^v\|\sin\beta_p - (d_{2,v} - d_{1,v}) \\ \vdots \\ \|\hat{\mathbf{X}}_{p,n_p}^v - \hat{\mathbf{X}}_{p,1}^v\|\sin\beta_p - (d_{n_p,v} - d_{1,v}) \end{bmatrix} \qquad (16)$$

The MLE of $\mathbf{p}$ can be obtained by solving the following problem,

$$\mathbf{p}^* = \arg\min_{\mathbf{p}} C_p(\mathbf{p})^{\mathrm{T}}\textstyle\sum_p^{-1}C_p(\mathbf{p}), \qquad (17)$$

where $\sum_p = diag(\sum_{X_{p,1}^v}, \ldots, \sum_{X_{p,n_p}^v}, \sum_{\tilde{x}_{p,1}^v}, \ldots, \sum_{\tilde{x}_{p,n_p}^v}, \sigma_{d,1}^2, \ldots, \sigma_{d,n_p}^2)$ is a block-wise diagonal matrix. $\sum_{X_{p,j}^v}$

and $\sum_{\tilde{x}_{p,j}^v}$ are the covariance matrices of $\mathbf{X}_{p,j}^v$ and $\tilde{\mathbf{x}}_{p,j}^v$, respectively. $\sigma_{d,j}^2$ is the estimation variance of $(d_{j,v} - d_{1,v})$.

With $\hat{\mathbf{X}}_{p,j}^v$, $\mathbf{l}_p$ and β_p obtained, we can compute $\mathbf{X}_{p,j}^W$ based on Lem. 2.

V. Experiments

We have implemented our algorithm using MATLAB under a PC. We use GSSI SIR-3000 GPR with 1.6 GHz antennas and the parameters are given as follows: the horizontal sample rate for the wheel encoder is 390 pulses per meter, the two-way travel time of the radar signal is 8 ns, the sample rate for the GPR is 1024 sample/scan. Each B-scan consists of 1643 A-scans on average. The camera used in the system is a 10 mega-pixel industry camera with model number DS-CFMT1000-H. The sensing suite shown in Fig. 2(a).

Since it is difficult to obtain the ground truth of the locations and sizes of the buried pipelines, we build a testbed platform so that we can place PVC pipes underneath. The platform is a raised square artificial floor with a side length of 5.5m and a height of 0.9m using wooden boards (see Fig. 2(b))). To emulate the reflection signals from metal pipes, we wrap each PVC pipe with aluminum foil. Before GPR scanning, we first create a global map using ORB-SLAM [17] that covers the entire field shown in Fig. 2(c). The ground truth is manually measured using a tape measure with 1.59mm accuracy.

In each setup, we change PVC pipe number and configurations. We have finished 5 sets of different pipe configurations. The pipe configurations and the corresponding pictures are shown in Fig. 7. Two types of pipes are used in our experiments, with radii being 4.62cm and 3.02cm, respectively. In each setup, we move the sensing suite along parallel GLTs in the grid to collect the camera and GPR data following the synchronization method in [20]. Each GLT generates a B-scan and 98 camera images on average. In each setup, we have at least 9 B-scans/GLTs.
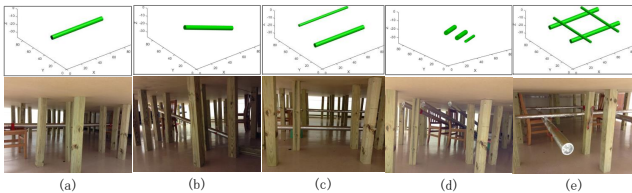

Fig. 7.   5 representative pipe configurations in experiments.

In our experiments, all pipelines are successfully detected. As for mapping quality, we first examine the orientation of the detected pipelines. As shown in Fig. 6, we adopt two angles α_p and β_p to describe pipe orientations where α_p is the angle between $\mathbf{l}_p$ and the X-axis of $\{W\}$. We define e_α and e_β to be the estimation errors of α_p and β_p, respectively. The values of e_α and e_β for each pipe are presented in Tab. I. The average values of e_α and e_β are $0.81°$ and $0.72°$, respectively. The maximum value of these two angle errors are $1.71°$ and $2.69°$, respectively. These small errors mean that the pipeline orientation estimation accuracy is satisfying.

TABLE I
ALL PIPELINE ORIENTATION ESTIMATION ERRORS ($°$).

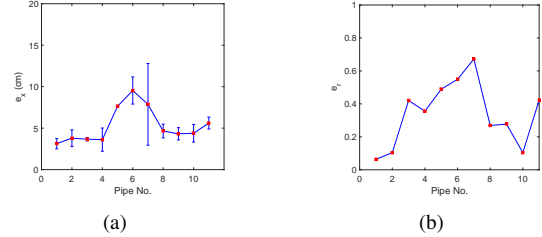| No.	pipe 1		pipe 2		pipe 3		pipe 4	
	e_α	e_β	e_α	e_β	e_α	e_β	e_α	e_β
1	0.54	0.48	—	—	—	—	—	—
2	0.46	2.69	—	—	—	—	—	—
3	1.34	0.19	0.01	0.44	—	—	—	—
4	1.71	0.64	0.40	0.51	0.27	1.37	—	—
5	1.16	0.47	1.62	0.47	0.74	0.19	0.61	0.48

Fig. 8.   Pipeline reconstruction results: (a) e_x statistics, and (b) Radius estimation relative error.

Next we examine the quality of the reconstructed center axis point $\mathbf{X}_{p,j}^W$ where we compute the Euclidean distance from $\mathbf{X}_{p,j}^W$ to the ground truth value of pipeline's centerline, denoted as error e_x. There are totally 11 pipes in our 5 experiment setups. We number them from 1 to 11 following the order of experiments. Fig. 8(a) presents the statistical results of e_x for each pipe, where the marker position is the average value and the vertical bars correspond to $[-\sigma, \sigma]$ with σ as the standard deviation. The overall average localization error is 4.69cm. Our pipeline localization algorithm is successful.

We define the metric $e_r = \frac{|\hat{r} - \bar{r}|}{\bar{r}}$ to evaluate the pipeline radius estimation results, where $\hat{r}$ and $\bar{r}$ are the radius estimation result and the corresponding ground truth value, respectively, and $|\cdot|$ denotes the absolute value operator. Fig. 8(b) presents the values of e_r for the 11 pipelines. The average value of e_r is 33.9%. The estimation errors are due to many factors, such as GPR accuracy limitation, hyperbola detection errors, the calibration error of GPR wave velocity, and the GPR scan localization errors. However, in most practical applications, the radii of pipelines are either prior known or conformal to typical standard sizes. As long as the result can assist finding the standard size, it is sufficiently accurate and acceptable.

VI. Conclusion and Future Work

We reported a novel subsurface pipeline mapping method by fusing GPR scans and camera images. The camera images and encoder readings were used to provide the global position for each GPR scan so that our algorithm can simultaneously map multiple lines without assuming perpendicular scanning. We derived a GPR sensing model that proves hyperbola formulation under GLTs. Then, we developed a multiple hyperbola extraction algorithm under the J-linkage framework to detect and classify the hyperbolas generated from multiple pipelines. Finally, we optimally estimated the orientations, radii and locations of all pipelines

by analyzing the extracted hyperbolas. We tested our method in 5 groups of physical experiments with representative pipeline configurations. The results showed that our method successfully reconstructed all subsurface pipes.

In the future, we will conduct more physical experiments and derive error analysis results. We also plan to further relax the constraint that requires the GPR to move linearly on flat ground by developing in-depth sensor fusion and GPR signal processing methods.

REFERENCES

[1] P. Zhang, X. Guo, N. Muhammat, and X. Wang, "Research on probing and predicting the diameter of an underground pipeline by gpr during an operation period," *Tunnelling and Underground Space Technology*, vol. 58, pp. 99–108, 2016.

[2] T. Hao, C. Rogers, N. Metje, D. Chapman, J. Muggleton, K. Foo, P. Wang, S. R. Pennock, P. Atkins, S. Swingler *et al.*, "Condition assessment of the buried utility service infrastructure," *Tunnelling and Underground Space Technology*, vol. 28, pp. 331–344, 2012.

[3] A. C. Royal, P. R. Atkins, M. J. Brennan, D. N. Chapman, H. Chen, A. G. Cohn, K. Y. Foo, K. F. Goddard, R. Hayes, T. Hao *et al.*, "Site assessment of multiple-sensor approaches for buried utility detection," *International Journal of Geophysics*, vol. 2011, 2011.

[4] M. A. González-Huici, I. Catapano, and F. Soldovieri, "A comparative study of gpr reconstruction approaches for landmine detection," *IEEE Journal of Selected Topics in Applied Earth Observations and Remote Sensing*, vol. 7, no. 12, pp. 4869–4878, 2014.

[5] R. Janning, A. Busche, T. Horváth, and L. Schmidt-Thieme, "Buried pipe localization using an iterative geometric clustering on gpr data," *Artificial Intelligence Review*, vol. 42, no. 3, pp. 403–425, 2014.

[6] C. Windsor, L. Capineri, P. Falorni, S. Matucci, and G. Borgioli, "The estimation of buried pipe diameters using ground penetrating radar," *Insight-Non-Destructive Testing and Condition Monitoring*, vol. 47, no. 7, pp. 394–399, 2005.

[7] W. Al-Nuaimy, Y. Huang, M. Nakhkash, M. Fang, V. Nguyen, and A. Eriksen, "Automatic detection of buried utilities and solid objects with gpr using neural networks and pattern recognition," *Journal of applied Geophysics*, vol. 43, no. 2-4, pp. 157–165, 2000.

[8] C. Maas and J. Schmalzl, "Using pattern recognition to automatically localize reflection hyperbolas in data from ground penetrating radar," *Computers & geosciences*, vol. 58, pp. 116–125, 2013.

[9] W. Li, H. Zhou, and X. Wan, "Generalized hough transform and ann for subsurface cylindrical object location and parameters inversion from gpr data," in *Ground Penetrating Radar (GPR), 2012 14th International Conference on*. IEEE, 2012, pp. 281–285.

[10] S. Li, H. Cai, D. M. Abraham, and P. Mao, "Estimating features of underground utilities: Hybrid gpr/gps approach," *Journal of Computing in Civil Engineering*, vol. 30, no. 1, p. 04014108, 2016.

[11] A. Fitzgibbon, M. Pilu, and R. B. Fisher, "Direct least square fitting of ellipses," *IEEE Transactions on pattern analysis and machine intelligence*, vol. 21, no. 5, pp. 476–480, 1999.

[12] E. Pasolli, F. Melgani, and M. Donelli, "Automatic analysis of gpr images: A pattern-recognition approach," *IEEE Transactions on Geoscience and Remote Sensing*, vol. 47, no. 7, pp. 2206–2217, 2009.

[13] Q. Dou, L. Wei, D. R. Magee, and A. G. Cohn, "Real-time hyperbola recognition and fitting in gpr data," *IEEE Transactions on Geoscience and Remote Sensing*, vol. 55, no. 1, pp. 51–62, 2017.

[14] A. Simi, S. Bracciali, and G. Manacorda, "Hough transform based automatic pipe detection for array gpr: Algorithm development and on-site tests," in *Radar Conference, 2008. RADAR'08. IEEE*. IEEE, 2008, pp. 1–6.

[15] H. Chen and A. G. Cohn, "Probabilistic robust hyperbola mixture model for interpreting ground penetrating radar data," in *Neural Networks (IJCNN), The 2010 International Joint Conference on*. IEEE, 2010, pp. 1–8.

[16] H. Chen and A. G, "Buried utility pipeline mapping based on multiple spatial data sources: a bayesian data fusion approach," in *IJCAI*, vol. 11. IEEE, 2011, pp. 2411–2417.

[17] R. Mur-Artal, J. M. M. Montiel, and J. D. Tardos, "Orb-slam: a versatile and accurate monocular slam system," *IEEE Transactions on Robotics*, vol. 31, no. 5, pp. 1147–1163, 2015.

[18] Y. Lu, D. Song, H. Li, and J. Liu, "Automatic recognition of spurious surface in building exterior survey," in *IEEE International Conference on Automation Science and Engineering Madison, Wisconsin, USA*, Aug. 2013.

[19] C. Chou, S.-H. Yeh, and D. Song, "Mirror-assisted calibration of a multi-modal sensing array with a ground penetrating radar and a camera," in *IEEE/RSJ International Conference on Intelligent Robots (IROS), Vancouver, Canada*, 2017.

[20] C. Chou, A. Kingery, D. Wang, H. Li, and D. Song, "Encoder-camera-ground penetrating radar tri-sensor mapping for surface and subsurface transportation infrastructure inspection," in *Robotics and Automation, 2018. ICRA'18. IEEE International Conference on*. Brisbane, Australia: IEEE, May 2018.

[21] F. Yang, X. Qiao, Y. Zhang, and X. Xu, "Prediction method of underground pipeline based on hyperbolic asymptote of gpr image," in *Ground Penetrating Radar (GPR), 2014 15th International Conference on*. IEEE, 2014, pp. 674–678.

[22] S. Shihab and W. Al-Nuaimy, "Radius estimation for cylindrical objects detected by ground penetrating radar," *Subsurface sensing technologies and applications*, vol. 6, no. 2, pp. 151–166, 2005.

[23] R. Toldo and A. Fusiello, "Robust multiple structures estimation with j-linkage," in *European conference on computer vision*. Springer, 2008, pp. 537–547.

[24] R. Hartley and A. Zisserman, *Multiple View Geometry in computer vision, 2nd Edition*. Cambridge Press, 2003.